HAL
open science

Single-sensor approach for impact localization and force reconstruction by using discriminating vibration modes

Dimitri Goutaudier, Didier Gendre, Véronique Kehr-Candille, Roger Ohayon

To cite this version:

Dimitri Goutaudier, Didier Gendre, Véronique Kehr-Candille, Roger Ohayon. Single-sensor approach for impact localization and force reconstruction by using discriminating vibration modes. Mechanical Systems and Signal Processing, 2020, 138, pp.106534. 10.1016/j.ymssp.2019.106534 . hal-02443465

HAL Id: hal-02443465

https://hal.science/hal-02443465v1

Submitted on 17 Jan 2020

HAL is a multi-disciplinary open access archive for the deposit and dissemination of scientific research documents, whether they are published or not. The documents may come from teaching and research institutions in France or abroad, or from public or private research centers.

L'archive ouverte pluridisciplinaire **HAL**, est destinée au dépôt et à la diffusion de documents scientifiques de niveau recherche, publiés ou non, émanant des établissements d'enseignement et de recherche français ou étrangers, des laboratoires publics ou privés.

Single-sensor approach for impact localization and force reconstruction by using discriminating vibration modes☆

Dimitri Goutaudier[a,b,c,*], Didier Gendre[b], Véronique Kehr-Candille[a], Roger Ohayon[c]

[a] *Onera, Department of Materials and Structures, Châtillon, France*
[b] *Airbus, Airport Operations, Blagnac, France*
[c] *Cnam, Structural Mechanics and Coupled Systems Lab., Paris, France*

Abstract

This study presents a novel strategy for identifying an impact event on a structure from vibration measurements. Compared to triangulation techniques that require at least three sensors on a plate-like structure, only one sensor is used in this work for localizing the impact point. The proposed approach consists in extracting specific modal ponderations as a signature of impact location. The force reconstruction problem is simultaneously addressed by fitting a parametric law. The proposed procedure captures the main load history parameters such as the impact time, its duration and its intensity. An impact test campaign is performed on a metallic plate, equipped with one accelerometer only, to confirm the validity of the proposed single-sensor approach. The methodology is efficient for accurately localizing impacts that are applied anywhere on the plate and for quickly estimating the main load history parameters.

Keywords: Structural Health Monitoring, impact identification, inverse problem, vibration analysis

1. Introduction

Reporting impact events is an important task of Structural Health Monitoring. It consists in localizing the impact point and in reconstructing the applied load history from indirect measurements of sensors distributed over the structure. Research is still ongoing to develop an impact identification technique that is accurate, robust, time efficient and that requires a low number of sensors. In the following, the reconstruction problem is presented before the localization problem.

The reconstruction problem is generally solved under the assumption of a linear elastic time invariant structure undergoing a point impact [1]. The load history is then linked to the vibration response by a convolution product with the impulse response of the structure. Therefore, the force reconstruction problem becomes a well-known deconvolution problem. This linear inverse problem is however poorly conditioned [2]. A direct inversion of the forward model may lead to a completely erroneous estimation due to noise contamination in the data or due to modelling errors. Mainly three regularization approaches have been developed, in time or frequency domain, to get a robust and accurate estimate of the solution.
Firstly, the Truncated Singular Values Decomposition (TSVD) consists in removing the small singular values of the transfer matrix [3, 4]. Leclère et al. [3] used the TSVD to reconstruct dynamic loads acting in an operating diesel engine. They investigated the influence of the truncation order on the quality of the reconstruction. If the truncation order was too high, the solution was unstable with a high norm ; if it was too small, the solution was stable but inaccurate. However, the choice of an appropriate truncation order may be time consuming. It can be done with the well-known L-curve method [5].

☆DOI of the published version: `https://doi.org/10.1016/j.ymssp.2019.106534`
*Corresponding author
Email address: `dimitri.goutaudier@gmail.com` (Dimitri Goutaudier)

Secondly, the Tikhonov regularization consists in a least-squares minimization that gives preference to a solution with desirable properties, such as a small norm [6, 7]. Boukria et al. [6] experimentally identified impacts applied on a circular aluminum plate equipped with four strain gauges. They employed the Tikhonov regularization technique with the L-curve method to select the regularization parameter. Their methodology is general but the L-curve method requires a high computation time since it consists in solving the reconstruction problem for many values of the regularization parameter.
Eventually, the reconstruction problem can be regularized by reducing the number of unknowns. Wang et al. [8] assumed that the impact duration was short enough in order to represent the impact as an impulse of unknown location and magnitude. Yan et al. [9] represented the load history with a half-sine to capture the impact intensity and the impact duration. They numerically validated their technique on a stiffened composite panel virtually equipped with 12 displacement sensors. Qiao et al. [10] assumed a decomposition of the load history in a basis of cubic B-splines. They accurately reconstructed impact forces applied at known locations on a clamped-free metallic plate.

The impact point coordinates are embedded in nonlinear terms of the vibration response through modal ponderations [11]. There are mainly four approaches to solve the nonlinear inverse problem of impact localization.
Firstly, triangulation techniques consist in distributing sensors over the structure to capture the Time Of Arrival (TOA) delays of elastic waves at sensor locations. Frieden et al. [12] used the TOAs of A_0 Lamb waves and a velocity model to identify the impact location. They experimentally validated their technique on a stiffened composite rectangular plate equipped with four FBG sensors. However, the velocity model was calibrated with a dense network of PZT sensors by applying many impacts on the structure, which may not be affordable in some applications. Zhao et al. [13] solved a non-linear set of equations to estimate impact location from the TOAs of A_0 Lamb waves. They experimentally validated their approach on a composite plate equipped with four strain gauges. However, their technique requires a large number of sensors if the structure is complex.
Secondly, sweeping techniques consist in solving the linear reconstruction problem on a grid of candidate impact points. The candidate that minimizes a distance between predictions and measurements is selected as the impact point. Li et al. [14] simultaneously identified the impact point and the load history applied on a clamped-free beam equipped with two accelerometers. The reconstruction problem was solved on a grid of evenly-spaced points with the Tikhonov regularization and the L-curve technique. The point that minimized a quadratic distance between predicted and measured data was selected as the impact point. Vladislav et al. [15] numerically validated the same technique with a Finite Element Model (FEM) of a homogeneous panel with a hole. The candidates were the nodes of the FEM mesh and they refined the localization results with an interpolation technique. El-Bakari et al. [16] used a Particle Swarm Optimization technique to select the candidate points to be tested. Their localization technique is based on Maxwell-Betti reciprocity theorem hence it does not depend on the load history. They numerically validated their methodology on a simply supported beam virtually equipped with three displacement sensors.
Thirdly, a few techniques are directly based on the estimation of the modal ponderations that embed the impact point coordinates. Briggs et al. [17] experimentally built a reference data set that indicated the modal ponderations depending on impact location. They experimentally validated their technique on a read/write head of a computer hard disk drive equipped with one accelerometer only. However, the number of modes to be kept in the analysis is not discussed and the impacts were applied at pre-defined locations. Wang et al. [8][18] proved that the modal ponderations involved in the vibration response are linked to the lines of the modal matrix. They used a least-squares procedure to simultaneously identify the impact intensity and the modal ponderations. These latter are then used to estimate the impact location with a Modal Assurance Criterion (MAC). They experimentally validated their technique on a simply supported beam equipped with one accelerometer only. However, their study is limited to the identification of a Dirac of unknown location and magnitude and the modes to be kept in the analysis are not indicated.
Eventually, non model-based techniques have been developed to avoid using a physical model. These techniques are based on neural networks and statistical methods [19][20]. However, significant training data-sets are required, which may not be affordable in some applications.

Previous studies show that numerous techniques have been proposed and validated on plate-like structures. However, at least three sensors are required for triangulating the impact location with the TOAs [6, 11, 12, 13, 21]. In this paper, a modal signature of the impact location is described instead of a time signature. It is proved that specific modal ponderations completely determine the impact point. A procedure is presented for estimating these modal ponderations from vibration measurements of a single sensor. The reconstruction problem is simultaneously solved by fitting a parametric law to capture the main load history parameters (the impact time, its duration and its intensity). The proposed approach is experimentally validated on a metallic plate equipped with one accelerometer only.

This paper is organized as follow. Section 2 presents the impact response model used for the impact identification. A procedure is described for identifying the model from the vibration measurements of a single sensor. Section 3 investigates the validity of the reverse link between the modal ponderations and the impact point. Section 4 is dedicated to the practical implementation of the proposed impact identification technique. Section 5 presents an experimental validation of the proposed single-sensor approach. Eventually, the results are discussed and improvements of the method are proposed in Section 6.

2. Governing response model for impact identification

Consider a plate-like structure and let S be the set of all the points of its geometry that are not blocked by the boundary conditions. Assume that the plate undergoes a transverse impact at some point $F \in S$ at time $t = 0$. Let $\psi(t)$ be the unit load history (maximum set to 1) and $f \neq 0$ be the impact intensity, so that $f\psi(t)$ represents the load history. Assume that $p \geq 2$ non-rigid vibration modes are known and that the structure is initially at rest (null initial conditions). The natural pulsation of the j-th mode is noted $\omega_{0j} > 0$ and its damping ratio is noted $\eta_j < 1$. The transverse vibration response $q(t)$ is considered at some point $C \in S$. Let's note $\phi_j(M)$ the j-th mass-normalized mode shape evaluated at some point $M \in S$ along the transverse direction. Assuming a modal behavior [22], the projection $\tilde{q}$ of q on the p known vibration modes is given by:

$$\tilde{q}(t) = \sum_{j=1}^{p} \phi_j(C)\phi_j(F) f h_j(t) \tag{1}$$

where $h_j(t) = (\psi * g_j)(t)$ denotes the convolution product between the unit load history and the impulse response of the j-th modal coordinate. This latter is defined by:

$$g_j(t) = \frac{1}{\omega_j} e^{-\eta_j \omega_{0j} t} \sin(\omega_j t) \tag{2}$$

with $\omega_j = \omega_{0j}\sqrt{1-\eta_j^2}$. In practice, accelerometers are generally more convenient than displacement sensors since they are smaller and they do not require a reference point. By derivating twice with respect to time, the acceleration response model $\tilde{a}(t)$ is given by:

$$\tilde{a}(t) = \sum_{j=1}^{p} \phi_j(C)\phi_j(F) f \ddot{h}_j(t) \tag{3}$$

It is important to notice that the response model (3) is only valid within the frequency band of the vibration modes considered in the analysis.

2.1. Images of the unknowns in the vibration response

By separating the terms depending on (C, ψ) from the terms depending on (F, f), equation (3) becomes:

$$\tilde{a}(t) = \ddot{\mathbf{L}}_{\psi}(t).\mathbf{Z_F} \tag{4}$$

where:

$$\ddot{\mathbf{L}}_{\psi}(t) = \Big(\phi_1(C)\ddot{h}_1(t) \ ... \ \phi_p(C)\ddot{h}_p(t)\Big) \tag{5}$$

$$\mathbf{Z_F} = f.(\phi_1(F) \ ... \ \phi_p(F))^T \tag{6}$$

$\ddot{\mathbf{L}}_{\psi}$ and $\mathbf{Z_F}$ are respectively the images of the unit load history $\psi(t)$ and the impulse parameters (F, f) in the vibration response. It can be appreciated that the response model (4) is linear with respect to $\ddot{\mathbf{L}}_{\psi}$ and $\mathbf{Z_F}$. Therefore, the identification of the images of the unknowns is a bilinear inverse problem.

The main advantage of this formalism is that $\ddot{\mathbf{L}}_{\psi}$ and $\mathbf{Z_F}$ can be simultaneously estimated from vibration measurements with a known procedure. The unit load history $\psi(t)$ is directly estimated in this procedure by fitting a parametric law (see sections 2.2 and 2.3). However, more theory is needed for the reverse link $\mathbf{Z_F} \mapsto (F, f)$. Section 3 is dedicated to this inverse problem.

2.2. Load history parametric law

It is well-known that bilinear inverse problems have an inherent scaling ambiguity [23]. Indeed, for any $\lambda \neq 0$:

$$\tilde{a}(t) = \lambda\ddot{\mathbf{L}}_{\psi}(t).\frac{1}{\lambda}\mathbf{Z_F} \tag{7}$$

The identity (7) results in the impossibility of identifying the true images $\ddot{\mathbf{L}}_{\psi}$ and $\mathbf{Z_F}$. To overcome this difficulty, we shall introduce an *a priori* knowledge on the unit impact load:

$$\psi = \psi(\boldsymbol{\alpha}) \tag{8}$$

where $\boldsymbol{\alpha} = (\alpha_1 \ ... \ \alpha_r)$ is a list of r parameters that completely describe the load history. These parameters may have a physical significance or not. In this study, three assumptions are made regarding the impact force profile:

- The sign of the load history remains constant,
- The impact duration is short enough to produce an oscillatory response,
- The load history exhibits a single peak.

Figure 1 shows four parametric laws that efficiently model an impact load history with the previous assumptions. The applicability of these laws for capturing the targeted load history parameters is discussed in section 5.4 through the experimental use-case.

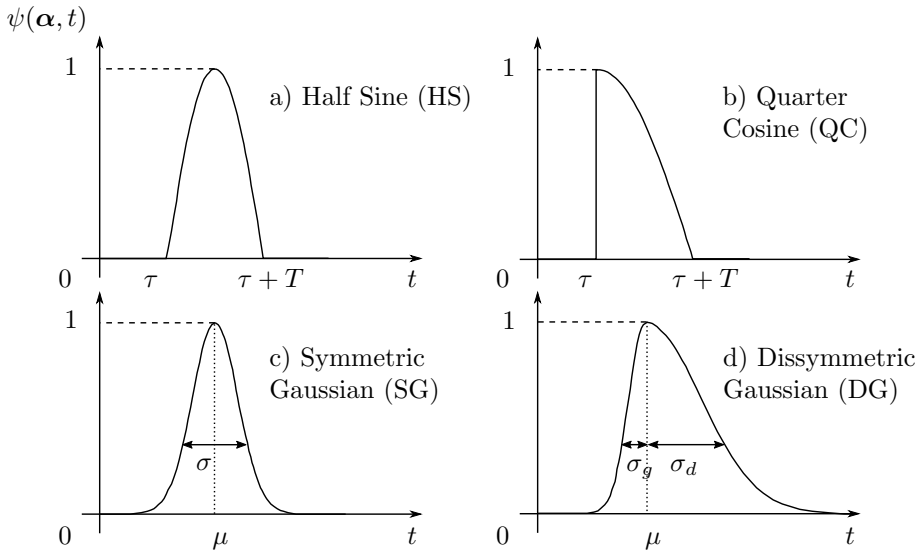

Figure 1: Parametric laws representing an impact force profile. a) Half Sine b) Quarter Cosine c) Symmetric Gaussian d) Dissymmetric Gaussian.

2.3. Model identification procedure

Let $\psi(\boldsymbol{\alpha})$ be the selected parametric law. Let $(a(t_i))_{1 \leq i \leq n}$ be n samples of the acceleration response measured at some point C of the structure (see section 4.2 for the sensor placement). Measurements are taken at times $t_i = i\Delta t$ with Δt the sampling period of the accelerometer. The problem is to estimate the load history parameters $\boldsymbol{\alpha}$ and the vector $\mathbf{Z_F}$ defined by equation (6). This can be done by minimizing a quadratic distance between predictions and measurements:

$$J(\boldsymbol{\alpha}, \mathbf{Z}) = \sum_{i=1}^{n} (\ddot{\mathbf{L}}_{\psi}(\boldsymbol{\alpha}, t_i).\mathbf{Z} - a(t_i))^2 \tag{9}$$

The proposed procedure to identify the model (4) by minimizing the relation (9) is as follow:

Step 1: Define a discrete variation interval V_i for each load parameter α_i.

Step 2: Explore the discretized load parameters space $V = \prod_{i=1}^{r} V_i$ by solving a linear least-squares problem for each $\boldsymbol{\alpha}^{(k)} \in V$:

$$\mathbf{Z}^{(k)} = \text{argmin}_{\mathbf{Z}} \; J(\boldsymbol{\alpha}^{(k)}, \mathbf{Z}) \tag{10}$$

Step 3: Select the couple $(\hat{\boldsymbol{\alpha}}, \hat{\mathbf{Z}}_{\mathbf{F}})$ that minimizes the cost function J.

Note that the dimension of each linear least-squares problem in Step 2 is $p \ll n$. Note also that each element of V is evaluated, but a more sophisticated exploration strategy could be considered to save computation time (see section 6.3). At the end of Step 3, the unit load history is estimated with the selected parametric law:

$$\hat{\psi} = \psi(\hat{\boldsymbol{\alpha}}) \tag{11}$$

A technique is presented in next section for estimating the impulse parameters (F, f) from their identified image $\hat{\mathbf{Z}}_{\mathbf{F}}$, which may be affected by an estimation error.

3. Impact localization from modal ponderations

Depending on impact location F, equation (6) shows that the p vibration modes are not excited in the same proportions through the terms $(\phi_j(F))_{1\leq j\leq p}$ called modal ponderations in the following. If the impact occurs at the modal node of the i-th mode, then it will not participate to the response: $\phi_i(F) = 0$. The impact intensity f does not change the proportions in which the modes are excited: it uniformly amplifies each modal ponderation. Consequently, $\mathbf{Z_F}$ is called the Amplified Modal Ponderation Vector (AMPV) in the following. The purpose of this section is to prove the validity of the reverse link $\mathbf{Z_F} \mapsto (F, f)$ when appropriate vibration modes are selected in the analysis.

3.1. 1D example: The simply supported metallic beam

To see how modal ponderations may link to the impact point, let's examine a simply supported beam undergoing an impact at some point F. From relation (6), the impact point F leads to the ponderations $Z_1 = f\phi_1(F)$ and $Z_2 = f\phi_2(F)$ in the vibration response. Inversely, assume that modal ponderations $(Z_1\ Z_2)$ are known. Figure 2 shows that two points could actually lead to Z_1: the true impact point F, and its symmetric F^* with respect to the center of the beam. However, the inspection of the second mode shape shows that an impact at F^* would lead to $(Z_1\ -Z_2)$. As a result, F^* can be discriminated, and impact point F is completely determined by the ponderations of the two first modes. (ϕ_1, ϕ_2) is called a discriminating modes family (see section 3.3).

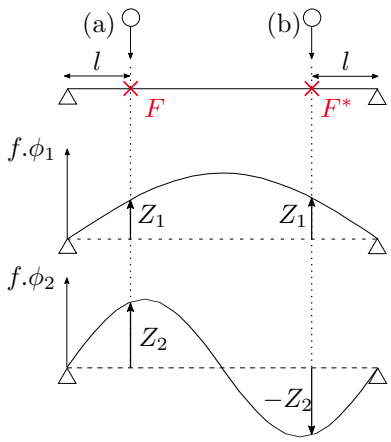

Figure 2: Bijective link $F \leftrightarrow \mathbf{Z_F} = (Z_1\ Z_2)^T$.

3.2. Iso-proportion lines

The previous reasoning on the 1D example can be extended to a plate-like structure as follow. Let's assume that the amplified modal ponderation vector $\mathbf{Z_F} \in \mathbb{R}^p$ associated to some impulse parameters (F, f) is known. The key step is to determine the impact points that would lead to the same image $\mathbf{Z_F}$ in the vibration response. To do so, let's introduce the following set of points:

$$L_{j/i}(\lambda) = \{M \in S \mid \phi_j(M) = \lambda\phi_i(M)\} \tag{12}$$

where λ is a real number. $L_{j/i}(\lambda)$ is called the λ iso-proportion line between modes j and i. It can be seen as an extension of the concept of nodal line defined by $L_j(0) = \{M \in S \mid \phi_j(M) = 0\}$.

To motivate this definition, assume that the impact occurred outside the nodal line of the first mode: $F \notin L_1(0)$. Then each modal ponderation can be expressed in terms of proportion with respect to the first mode:

$$\mathbf{Z_F} \propto (1\ \lambda_{21}\ ...\ \lambda_{p1})^T \tag{13}$$

with:

$$\lambda_{j1} = \frac{\phi_j(F)}{\phi_1(F)} \tag{14}$$

Note that each modal proportion λ_{j1} is known since it is the ratio between the j-th and the first coordinate of the AMPV. It is now clear that the impact occurred at an intersection point of iso-proportion lines:

$$F \in \cap_{j=2}^{p} L_{j/1}(\lambda_{j1}) \tag{15}$$

In general, the case $\mathbf{Z_F} = \mathbf{0}$ may occur and the following set of points must be introduced:

$$I(F) = \begin{cases} \cap_{j=1}^{p} L_j(0) & \text{if } \phi_j(F) = 0 \text{ for any } j \in [\![1, p]\!] \\ \cap_{j=1, j\neq i}^{p} L_{j/i}(\lambda_{ji}) & \text{if } \phi_i(F) \neq 0 \text{ for some } i \in [\![1, p]\!] \end{cases} \tag{16}$$

Then the general localization property of the impact point becomes:

$$F \in I(F) \tag{17}$$

Note that relation (17) is independent from the impact intensity f since we are working with proportions.

3.3. Discriminating Modes Family (DMF)

It is remarkable that the iso-proportion lines may have a unique intersection point (see section 3.4):

$$I(F) = \{F\} \tag{18}$$

In this case, it is said that $\mathcal{F} = (\phi_j)_{1\leq j\leq p}$ is a Discriminating Modes Family (DMF) for the point $F \in S$. If this property holds for any $F \in S$, then it is said that $\mathcal{F}$ is global DMF of the structure.

For a plate-like structure, it can be shown that at least three vibration modes should be kept in the analysis to form a global DMF [24]:

$$p \geq 3 \tag{19}$$

The basic idea behind relation (19) is that the impact point is located by two coordinates. Since one vibration mode is kept as a reference to define the modal proportions (14), two other vibration modes should at least be considered to intersect two iso-proportion lines at the impact point only.

3.4. 2D application: The simply supported metallic plate

Consider a simply supported metallic plate with dimensions $a \times b$. From [25], the (i, j) mass-normalized flexural mode shape of such a plate is:

$$\phi_{i,j}(x, y) \propto \sin\left(\frac{i\pi x}{a}\right) \sin\left(\frac{j\pi y}{b}\right) \tag{20}$$

Let $S =]0, a[\times]0, b[$ be the set of all the points of the plate that are not blocked by boundary conditions. Let $F = (x_F\ y_F) \in S$ be a point of the plate undergoing a transverse impact. Let's note $\phi_1 = \phi_{1,1}, \phi_2 = \phi_{1,2}$, and $\phi_3 = \phi_{2,1}$ (see Figure 3a). It is straightforward to show:

$$L_{2/1}(\lambda_{21}) = \{(x, y) \in S \mid y = y_F\} \tag{21}$$

$$L_{3/1}(\lambda_{31}) = \{(x, y) \in S \mid x = x_F\} \tag{22}$$

Thus the iso-proportion lines intersect at impact location only (see Figure 3b). Therefore, (ϕ_1, ϕ_2, ϕ_3) is a global DMF of the plate.

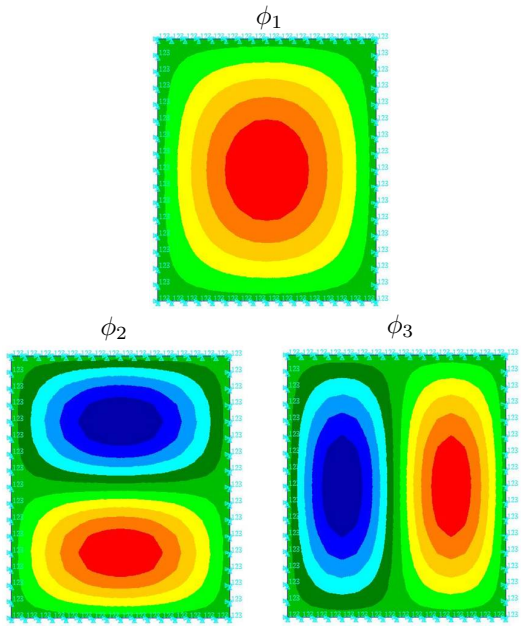

(a) Mode shapes of the global DMF (ϕ_1, ϕ_2, ϕ_3).

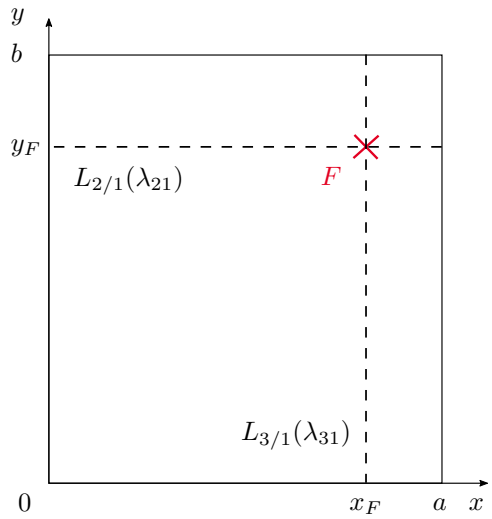

(b) Iso-proportion lines intersecting at impact location only.

Figure 3: Analytical study of a simply supported plate

4. Implementation

From previous section, the reverse link between the AMPV and the impulse parameters holds if discriminating vibration modes are selected in the analysis. In practice, however, mode shapes are not analytically known hence iso-proportion lines cannot be explicitly derived. Instead, mode shapes are evaluated, experimentally or numerically, along a finite number of Degrees Of Freedom (DOF). The purpose of this section is to propose a practical technique for estimating the impulse parameters (F, f) from an estimation of the AMPV $\hat{\mathbf{Z}}_\mathbf{F}$ by using discretized mode shapes. The final impact identification procedure is then presented.

Let $\phi_\mathbf{j} \in \mathbb{R}^N$ be the j-th discretized mode shape evaluated along N unblocked transverse DOFs. Therefore a $N \times p$ modal matrix $\mathbf{\Phi}$ is available. Let's note $\phi^*_\mathbf{i}$ the i-th column of $\mathbf{\Phi}^T$ so that:

$$\mathbf{\Phi}^T = [\phi^*_\mathbf{1}|...|\phi^*_\mathbf{N}] \tag{23}$$

To simplify, the index refering to the impacted transverse DOF is abusively noted $F \in [\![1, N]\!]$. Consequently, the AMPV is given by:

$$\mathbf{Z}_\mathbf{F} = f.\phi^*_\mathbf{F} \tag{24}$$

It is remarkable that if the modal matrix is truncated on a DMF for the point $F \in S$, then the corresponding impacted DOF is bijectively linked to $\mathbf{Z}_\mathbf{F}$ (see section 3.3). Consequently, only the column of $\mathbf{\Phi}^T$ with index $F \in [\![1, N]\!]$, namely $\phi^*_\mathbf{F}$, is exactly collinear to $\mathbf{Z}_\mathbf{F}$. The impact intensity f is then the collinearity factor between $\mathbf{Z}_\mathbf{F}$ and $\phi^*_\mathbf{F}$.

4.1. Collinearity research procedure

In practice, the AMPV is always affected by an estimation error:

$$\hat{\mathbf{Z}}_\mathbf{F} = \mathbf{Z}_\mathbf{F} + \mathbf{e} \tag{25}$$

The error term $\mathbf{e} \in \mathbb{R}^p$ may be due to some noise contiminating the data or due to modelling errors in (3). In particular, it is likely that the impact does not occur at a DOF at which the mode shapes have been evaluated. Consequently, $\hat{\mathbf{Z}}_\mathbf{F}$ might not be exactly collinear to $\phi^*_\mathbf{F}$. Hence the impacted DOF cannot be identified by looking for the only column of $\mathbf{\Phi}^T$ that is collinear to the estimated AMPV. Instead, we shall look for the columns of $\mathbf{\Phi}^T$ that are the most collinear to $\hat{\mathbf{Z}}_\mathbf{F}$.

To do so, let's define the angle between two vectors $\mathbf{u}$ and $\mathbf{v}$ by the small angle $\theta \in [0, \pi/2]$ between $\mathbf{v}$ and $\text{span}\,(\mathbf{u})$. Let $\epsilon > 0$ be a proximity tolerance and M be an arbitrary point of the structure associated to one of the evaluated DOFs. Let's note $\phi^*_\mathbf{M}$ the associated column of $\mathbf{\Phi}^T$ and let θ_M be the angle between $\phi^*_\mathbf{M}$ and $\phi^*_\mathbf{F}$. By continuity arguments, it exists a collinearity tolerance $\theta_\epsilon(F)$ such that $\theta_M < \theta_\epsilon(F)$ implies $\|M - F\| \leq \epsilon$ (see Figure 4).

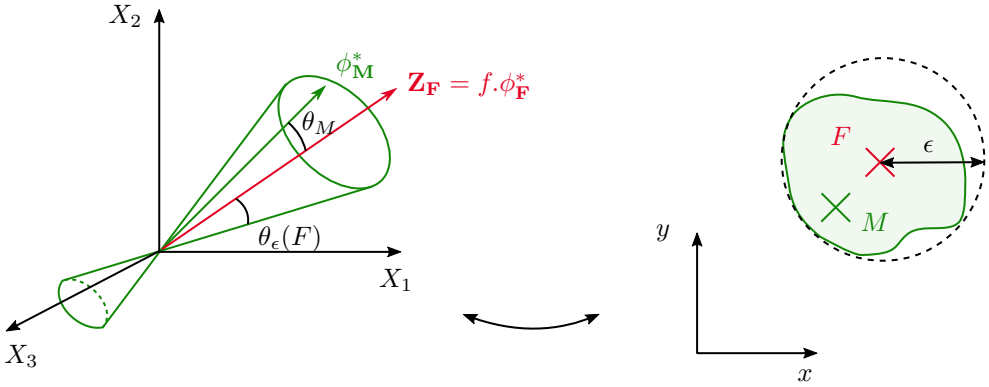

Figure 4: Conversion of the proximity tolerance ϵ into a collinearity tolerance $\theta_\epsilon(F)$.

Consequently, an adaptive collinearity tolerance should be used since there might be important discrepancies in the values of θ_ϵ depending on the areas of the structure (see example in section 6.2). This can be achieved by introducing a dispersion factor γ as follow:

Inputs : $\mathbf{\Phi}$, $\hat{\mathbf{Z}}_\mathbf{F}$, $\gamma \geq 1$

Step 1: Compute the angles $\hat{\theta}_i$ between the estimated AMPV $\hat{\mathbf{Z}}_\mathbf{F}$ and the vectors $\phi^*_\mathbf{i}$.

Step 2: Compute $\hat{\theta}_m = \min_i \hat{\theta}_i$.

If $\hat{\theta}_m > \max \theta_\epsilon$ then the identification failed. Else:

Step 3: Identify $I \subset [\![1, N]\!]$ such that $\hat{\theta}_i \leq \gamma \hat{\theta}_m$ for any $i \in I$.

Step 4: Associate a point $F_i \in S$ for each $i \in I$.

Step 5: Compute the collinearity factors for each $i \in I$:

$$f_i = \frac{(\phi^*_\mathbf{i})^T . \hat{\mathbf{Z}}_\mathbf{F}}{\|\phi^*_\mathbf{i}\|_2^2} \tag{26}$$

Outputs: Set of impulse parameters candidates (F_i, f_i)

The motivation for the conditional statement between Steps 2 and 3 is to alert from obvious incorrect identifications (the localization error would necessarily be greater than ϵ). Note that if $\|\mathbf{e}\|_2$ is small enough, or more generally if $\mathbf{e}$ is properly oriented, then $\hat{\mathbf{Z}}_\mathbf{F}$ is almost collinear to $\boldsymbol{\phi}^*_\boldsymbol{F}$: $\hat{\theta}_F \approx 0$. Each candidate $F_i \in S$ is then ϵ-close to the true impact point $F \in S$ if:

$$\hat{\theta}_i + \hat{\theta}_F \leq \theta_\epsilon(F) \tag{27}$$

4.2. Sensor placement on a neutral point

The robustness of the AMPV estimation can be increased with an adequate sensor placement as follow. Each linear least-squares problem (10) is solved by inverting a $p \times p$ matrix $\mathbf{A}(\boldsymbol{\alpha}^{(k)}, C)$ given by:

$$\mathbf{A}(\boldsymbol{\alpha}^{(k)}, C) = \sum_{i=1}^{n} \ddot{\mathbf{L}}_{\psi}(\boldsymbol{\alpha}^{(k)}, t_i)^T . \ddot{\mathbf{L}}_{\psi}(\boldsymbol{\alpha}^{(k)}, t_i) \tag{28}$$

It is a remarkable property that its condition number in 2-norm can be bounded as follow [24]:

$$\kappa(\boldsymbol{\alpha}^{(k)}, C) \leq M(\boldsymbol{\alpha}^{(k)}). \max_{i,j} \left| \frac{\phi_j(C)}{\phi_i(C)} \right|^2 \tag{29}$$

Therefore the majoration (29) can be decreased by selecting a sensor placement $C \in S$ such that

$$\nu(C) = \max_{i,j} \left| \frac{\phi_j(C)}{\phi_i(C)} \right|^2 \tag{30}$$

is minimal. From a physical point of view, if $\nu(C) = 1$ then the sensor location does not affect the error amplification by inverting the matrices $\mathbf{A}(\boldsymbol{\alpha}^{(k)}, C)$. Such sensor locations, if they exist, are called neutral points of the selected vibration modes family. For instance, the global DMF $(\phi_{1,1}, \phi_{1,2}, \phi_{2,1})$ of the simply supported plate has four neutral points (see Figure 5).

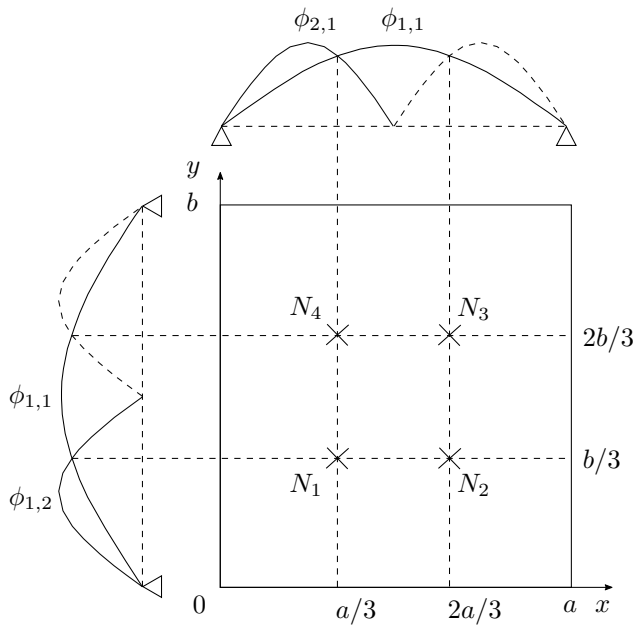

Figure 5: Neutral points of the global DMF $(\phi_{1,1}, \phi_{1,2}, \phi_{2,1})$ of the simply supported plate.

4.3. Final procedure

The program flowchart of the proposed impact identification technique is presented in Figure 6. The selection of a DMF is performed by computing θ_ϵ for each DOF at which the mode shapes have been evaluated. As a rule of thumb, the minimum of θ_ϵ should be greater than 3-4° to resist estimation errors on $\mathbf{Z_F}$. However, the number of modes kept in the analysis should not be too high to prevent a poor conditionning of the matrices $\mathbf{A}$ (see section 4.2).

An approximate value of θ_ϵ can be computed for each evaluated DOF as follow. Let M be an evaluated DOF and θ_0 be an initial collinearity tolerance. Then look for all the $\phi_\mathbf{i}^*$ making a small angle (see section 4.1) with $\phi_\mathbf{M}^*$ lower or equal than θ_0. If all the points attached to the DOFs associated to the identified $\phi_\mathbf{i}^*$ are ϵ-close to the point M then repeat the procedure with a larger collinearity tolerance; else reduce the collinearity tolerance. The approximate value of $\theta_\epsilon(M)$ is the maximum admissible collinearity tolerance found with this procedure.

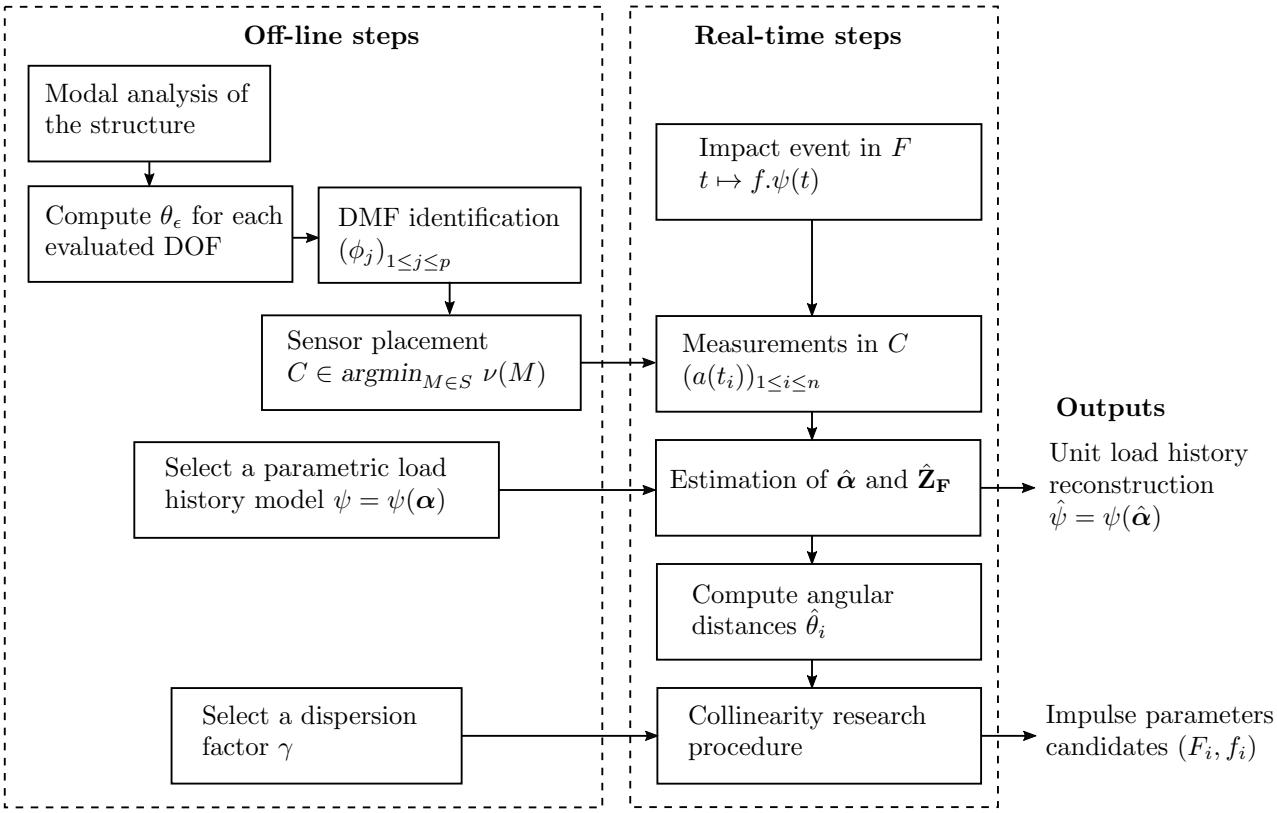

Figure 6: Program flowchart of the impact identification technique.

5. Experimental validation on a simply supported plate

The impact identification technique presented in previous section can theoretically work with a single measurement point. The purpose of this section is to experimentally validate the developed methodology on a rectangular simply supported plate equipped with one accelerometer only. The main advantage of this academic structure is to ease the modal analysis step of the procedure (see Figure 6). However, the structure's geometry and the anisotropy of its constitutive materials are not obstacles for the proposed approach, as long as equation (4) can be used. The structure's complexity is indeed fully embedded in the vibration modes that can be determined either experimentally or numerically.

5.1. Set-up

The experimental set-up consists in a rectangular aluminum plate mounted on a specific support that reproduces simply supported boundary conditions (see Figure 7). The details of the set-up are described in [26] and plate properties are summarized in Table 1. The accelerometer 352C22 PCB Piezotronics is glued near the neutral point $N_1 = (a/3, b/3)$ during the whole tests (see Figure 5) . Impacts are applied with different heads of a hand-held impact hammer IH-02 Tenlee Piezotronics (rubber, nylon, aluminum and steel). Impact load history and acceleration data are recorded with the software m+p Analyzer Rev 5.1, with a sampling frequency of 12.8kHz and a measurement duration of 0.64s.

A Finite Element Model (FEM) of the plate is created with Nastran 2014 to compute the first six flexural mode shapes of the plate. The FEM consists in a plate discretized in 8×8 CQUAD8 elements, allowing a spatial resolution for the localization problem of $\min(a, b)/16 = 2.25$ cm. The number of unblocked transverse DOFs is $N = 161$.

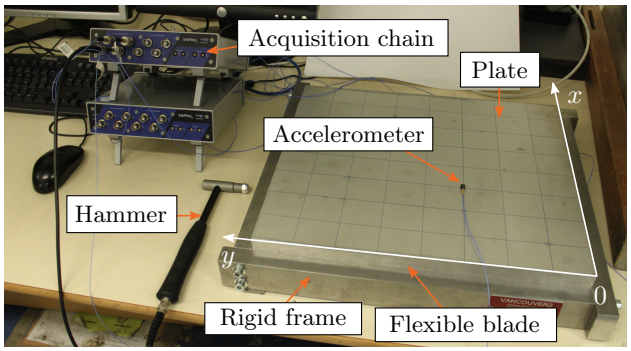

Figure 7: Experimental set-up.

Dimensions	$a = 36$cm, $b = 42$cm, $h = 3$mm
Material	Al 2017
Density	2800 kg.m^{-3}
Young modulus	72.5 GPa
Poisson ratio	0.33
Mode 1	$f_{01} = 94.7$Hz, $\eta_1 = 1\%$
Mode 2	$f_{02} = 224$Hz, $\eta_2 = 0.3\%$
Mode 3	$f_{03} = 269$Hz, $\eta_3 = 0.6\%$
Mode 4	$f_{04} = 391$Hz, $\eta_4 = 0.3\%$
Mode 5	$f_{05} = 430$Hz, $\eta_5 = 0.09\%$
Mode 6	$f_{06} = 547$Hz, $\eta_6 = 0.14\%$

Table 1: Plate properties and results of an experimental modal analysis.

5.2. Methodology

The impact identification methodology is as follow. Each impact is applied at the center of one of the cells marked on the plate (see Figure 7). Soft or hard impacts are applied by changing the tip of the impact hammer (rubber, nylon, aluminum and steel). The plate is initially at rest before each impact. The signal processing technique is then divided in five steps:

Step 1: The instant of impact is estimated with a threshold technique on the acceleration measurements:

$$t_0 = \text{argmin}_{t_i} \ \{|a(t_i)| > 0.05 \times \max |a(t_i)|\} \tag{31}$$

Step 2: The signal length is reduced from the time zero point to capture ten oscillations of the first vibration mode:

$$D = 10/f_{01} \tag{32}$$

Step 3: The semi-linear least-squares procedure described in section 2.3 is used to estimate both the load history parameters $\hat{\boldsymbol{\alpha}}$ of the selected parametric law and the AMPV $\hat{\mathbf{Z}}_{\mathbf{F}}$.

Step 4: The collinearity research procedure described in section 4.1 is used to identify impulse parameters candidates (F_i, f_i) from $\hat{\mathbf{Z}}_{\mathbf{F}}$.

Step 5: Since the curvature of the plate is null, the estimated impact location $\hat{F} \in S$ and the estimated impact intensity $\hat{f}$ are derived from the candidates (F_i, f_i) as follow:

$$\begin{pmatrix} \hat{F} \\ \hat{f} \end{pmatrix} = \sum_{i \in I} w_i \begin{pmatrix} F_i \\ f_i \end{pmatrix} \tag{33}$$

where the weights give more importance to candidates associated to small angles:

$$w_i = \cos(\hat{\theta}_i) / \sum_{k \in I} \cos(\hat{\theta}_k) \tag{34}$$

A localization is considered successful if the estimated impact point $\hat{F}$ is within a distance $\epsilon = 3.6$cm of the true impact point F (half of a cell diagonal). Figure 8 illustrates Steps 4 and 5 leading to a successful localization. In this example, the global DMF the plate (ϕ_1, ϕ_2, ϕ_3) is used in the analysis hence the dimension of the vectors $\phi^*_{\mathbf{i}}$ is 3.

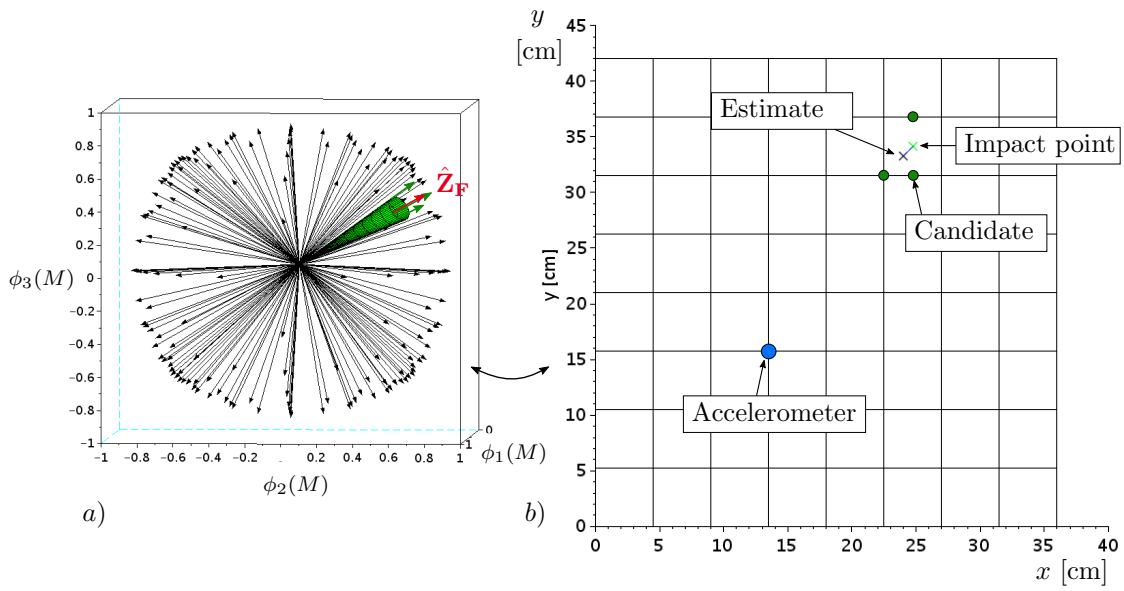

Figure 8: Illustration of the localization procedure. a) Collinearity research cone (red arrow: $\hat{\mathbf{Z}}_\mathbf{F}$, black arrows: $\phi_\mathbf{i}^*$). b) Successful localization of the impacted cell.

5.3. Localization results

The HS parametric law (see Figure 1) is selected to display the localization results. The influence of the hammer tip and the modes selected in the analysis is investigated. Four vibration modes families are considered: $\mathcal{F}_1 = (\phi_1, \phi_2, \phi_3)$, $\mathcal{F}_2 = (\mathcal{F}_1, \phi_4)$, $\mathcal{F}_3 = (\mathcal{F}_2, \phi_5)$, and $\mathcal{F}_4 = (\mathcal{F}_3, \phi_6)$. Table 2 summarizes the parameters of the procedure.

Table 3 and Figures 9a) to 9d) present the localization results of the impact tests. A green cross represents an impact point, the linked black cross is the associated estimate, and a red cross is displayed if no estimate is found. Most of the impacts applied with the rubber tip are successfully localized within the proximity tolerance by using $\mathcal{F}_1$ (94% success). Adding more modes in the analysis deteriorates the localization performances (success rate drops to 33%). The opposite happens with the other tips. The best localization performances are reached by keeping more modes in the analysis, namely by using $\mathcal{F}_4$. These results are discussed in sections 6.1 and 6.2.

In total, 93% of the applied impacts (239/256) are successfully localized, as long as appropriate modes are kept in the analysis. Thus the single-sensor approach is validated for localizing soft and hard impacts applied at any point of the plate.

Cell dimensions	$a_e = a/8, b_e = b/8$
Proximity tolerance	$\epsilon = (a_e^2 + b_e^2)^{1/2}/2 = 3.6$cm
Signal length	$D = 0.105$s
Sampling frequency	$f_e = 1/\Delta t = 12.8$kHz
Accelerometer position	$(3a_e, 3b_e)$
Available modes	$(\phi_1, ..., \phi_6)$
Dispersion factor	$\gamma = 2$
Load history model	Half Sine (HS)
Impact parameters space	$[T_{min}, T_{max}] = [0.3, 6]$ms
	$\Delta T = 0.1$ms

Table 2: Parameters for the impact identification procedure.

Hammer tip	$\mathcal{F}_1$	$\mathcal{F}_2$	$\mathcal{F}_3$	$\mathcal{F}_4$
Rubber	60(94%)	34	23	21
Nylon	49	56	57	58(91%)
Aluminum	43	49	57	62(97%)
Steel	44	53	57	59(92%)

Table 3: Number of localizations (/64) within the proximity tolerance (best success rate in parenthesis).

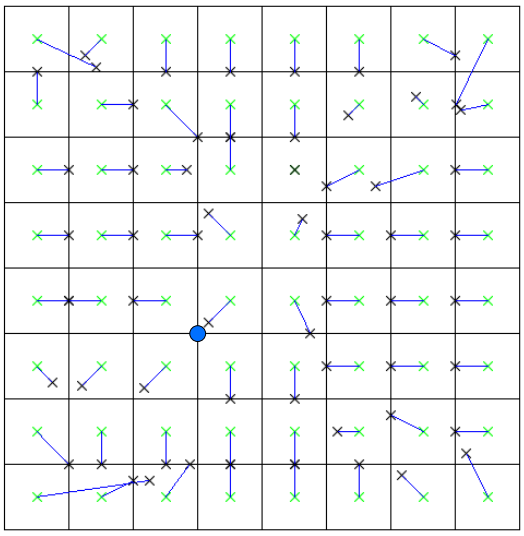

a) Rubber, $\mathcal{F}_1$

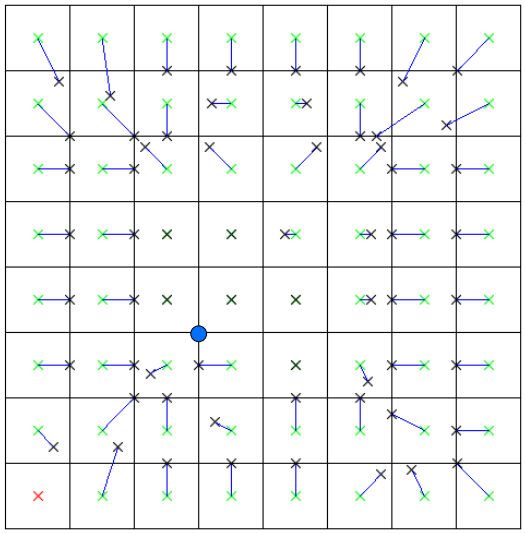

b) Nylon, $\mathcal{F}_4$

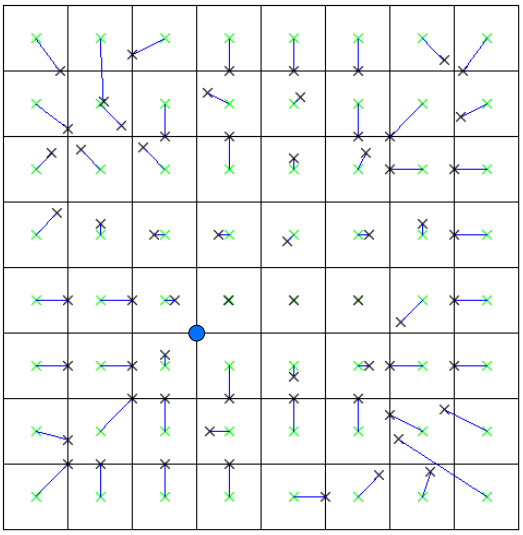

c) Aluminum, $\mathcal{F}_4$

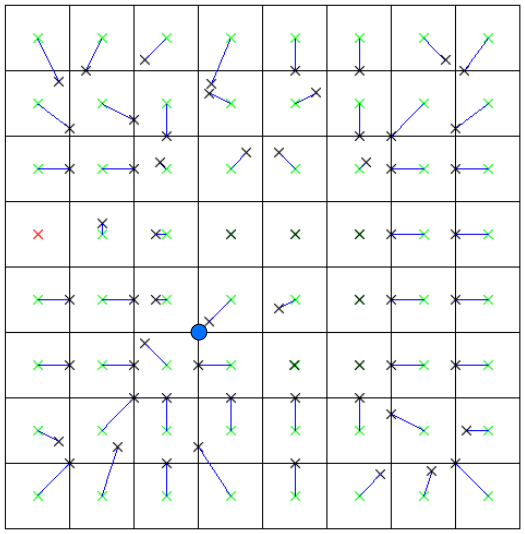

d) Steel, $\mathcal{F}_4$

Figure 9: Localization maps depending on hammer tip.

5.4. Load history reconstruction results

The influence of the parametric law on the force reconstruction performances is investigated through two use-cases:

Soft impact: Smooth one-peak load history applied with the rubber tip at $F = (4.5a/8, 2.5b/8)$,

Hard impact: Spiky multi-peaks load history applied with the steel tip at $F = (1.5a/8, 3.5b/8)$.

The four parametric laws presented in Figure 1 are tested for reconstructing the applied forces. With HS and QC models, the instant of impact is detected with the trigger technique (31) only. With SG and DG models, the instant of impact is refined in the semi-linear least-squares procedure with the peak position parameter μ. Table 3 presents the impact parameters space depending on the load history model. The other parameters of the procedure are the same as in Table 2.

HS & QC	SG	DG
$T_{min} = 0.3$ms $T_{max} = 6$ms $\Delta T = 0.1$ms	$\mu_{min} = -5\Delta t$ $\mu_{max} = +30\Delta t$ $\Delta\mu = \Delta t$ $\sigma_{min} = 0.01$ms $\sigma_{max} = 1$ms $\Delta\sigma = 0.05$ms	$\mu_{min} = -5\Delta t$ $\mu_{max} = +30\Delta t$ $\Delta\mu = \Delta t$ $\sigma_g^{min} = \sigma_d^{min} = 0.01$ms $\sigma_g^{max} = \sigma_d^{max} = 1$ms $\Delta\sigma_g = \Delta\sigma_d = 0.05$ms

Table 4: Impact parameters space depending on the load history model ($\Delta t = 1/f_e$).

Reconstruction of the soft impact

Figure 10 shows the reconstruction results by using the vibration modes family $\mathcal{F}_1$. Table 5 indicates the localization performances, the force reconstruction error (relative distance in 2-norm between measured and predicted data), the estimated intensity, and the associated set of estimated parameters.

The force reconstruction error is much larger with QC model ($> 100\%$). The initial vertical slope of this model is not adapted for this smooth load history. Hence the impact time is estimated too early with the trigger technique. As a result, candidate impact points are found too far (within 3ϵ), and impact intensity is overestimated to compensate the localization error. The best predictions are obtained with DG model which captures the slight dissymmetry of the peak (13.9% of relative error).

Figure 11 shows the reconstruction of the acceleration data depending on the load history model selection. Each model almost equally reconstructs measured data (relative error $\approx 30\%$). However, Figure 12 shows that predicted data with QC model are in advance with respect to the other models. It is due to the early estimation of the impact time described above.

Predictions	HS	QC	SG	DG
Localization	$\leq \epsilon$	$\leq 3\epsilon$	$\leq \epsilon$	$\leq \epsilon$
Intensity estimate	11.8N	24.2N	13.1N	12.8N
Reconstruction error	24.4%	132%	23.3%	13.9%
Estimated impact shape parameters	$\hat{T} = 2.9$ms	$\hat{T} = 4.3$ms	$\hat{\mu} = +18\Delta t$ $\hat{\sigma} = 0.7$ms	$\hat{\mu} = +15\Delta t$ $\hat{\sigma_g} = 0.58$ms $\hat{\sigma_d} = 1$ms

Table 5: Identification of the soft impact depending on the load history model selection.

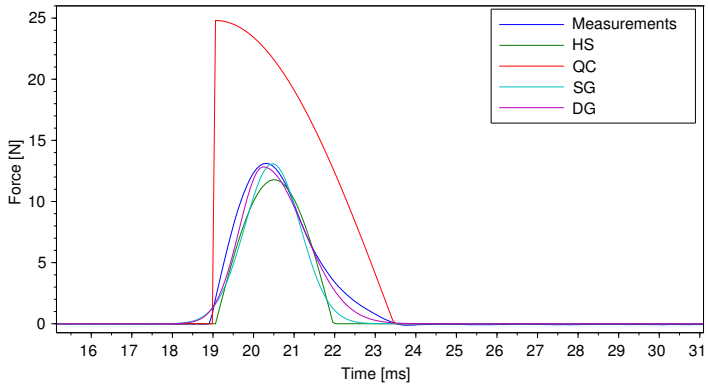

Figure 10: Force reconstruction of the soft impact.

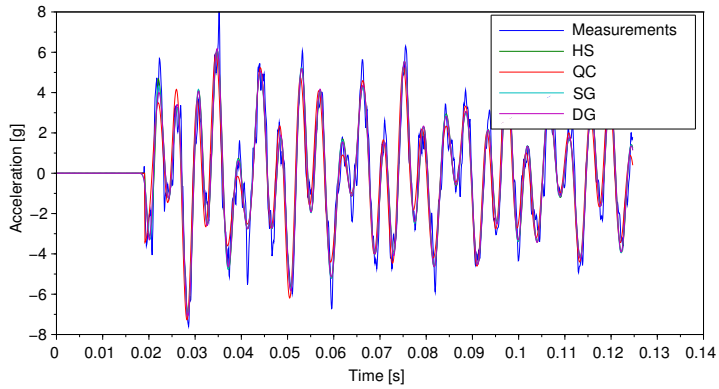

Figure 11: Acceleration reconstruction with the soft impact.

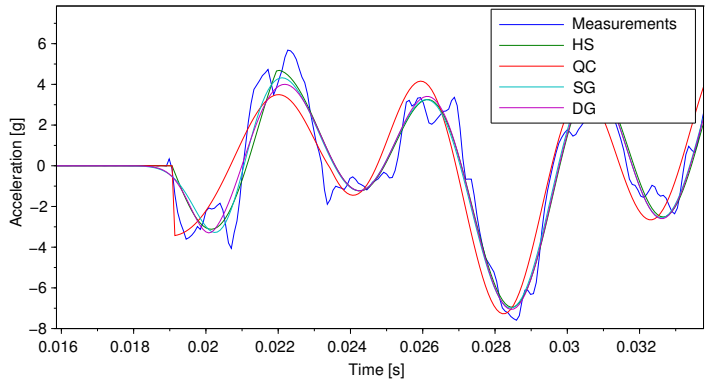

Figure 12: Close view of the acceleration data reconstruction near the impact time.

Reconstruction of the hard impact

The same methodology is applied with $\mathcal{F}_4$ to identify the hard impact. HS and QC model successfully localize the impact, and roughly capture the main peak of the load history (see Table 6 and Figure 13).

However, SG and DG models do not identify the impact (zero candidate is found). The peak position estimation is $\hat{\mu} = 30\Delta t$, which is at the border of the variation interval of this parameter (see Table 4). It is observed that the distance (9) is more reduced by delaying the impact time, thus by adding zeros in predicted data. The main peak impact duration might be too small ($<$ 1ms) to be represented by the smooth SG and DG profiles. Therefore the impact parameters space is inappropriate to reconstruct the applied load history with these models.

Figure 14 shows the reconstruction of the acceleration data with HS and QC models. The relative error between predicted and measured acceleration data is high ($>$ 90%). This can be explained as follow. The impact duration is much lower with the steel tip thus higher order modes are excited. The six first modes of the plate are not dominant in the response, hence only the low frequency content of the vibration response is reconstructed. However, note that the reconstruction of the acceleration data is not the objective of an impact identification technique.

Predictions	HS	QC
Localization	$\leq \epsilon$	$\leq \epsilon$
Intensity estimate	20.5N	15.6N
Reconstruction error	69%	64%
Estimated impact shape parameters	$\hat{T} = 0.8$ms	$\hat{T} = 1.1$ms

Table 6: Identification of the hard impact depending on the load history model selection.

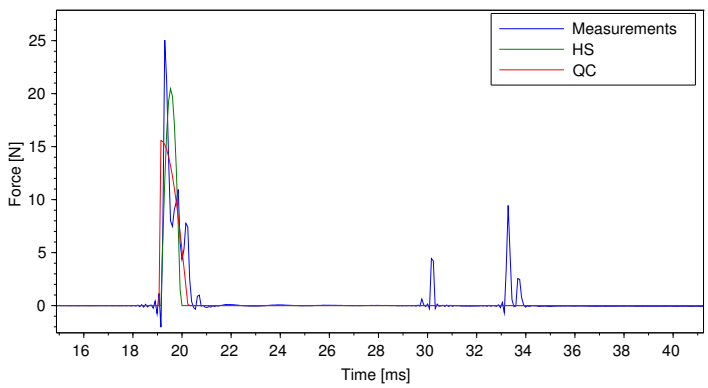

Figure 13: Force reconstruction of the hard impact.

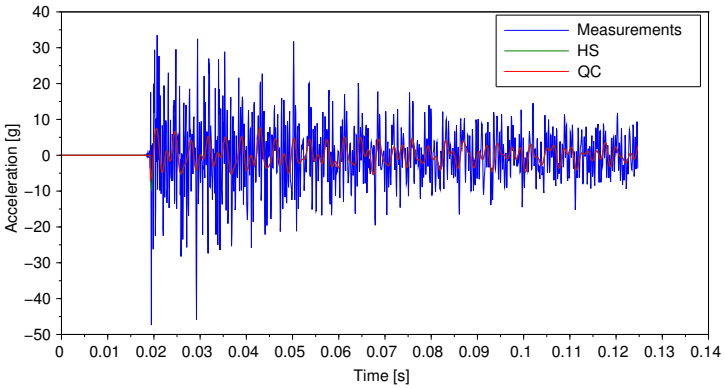

Figure 14: Acceleration reconstruction with the hard impact.

6. Discussion

The purpose of this section is to explain the experimental results and to propose improvements of the method presented in this work.

6.1. Trade-off accuracy/robustness on the modal ponderations estimation

Table 3 shows that more than 90% of applied impacts are localized within the proximity tolerance, as long as appropriate modes are selected in the analysis. With the rubber tip, the best results are obtained with $\mathcal{F}_1$, while adding modes seems to deteriorate the localization performances. The opposite is observed with the other tips. Two examples are described in the following to illustrate this phenomenon.

Figure 15 shows the frequency contents of measured and predicted acceleration data for a soft impact applied with the rubber tip. It can be seen that the frequency band [85,285]Hz is correctly reconstructed, meaning that the modal ponderations of ϕ_1, ϕ_2 and ϕ_3 are accurately estimated. Hence the impact is accurately localized as well given that $\mathcal{F}_1 = (\phi_1, \phi_2, \phi_3)$ is a global DMF of the plate (see section 3.4). However, it is observed that the ponderation of ϕ_6 is inaccurately estimated by using $\mathcal{F}_4$. The estimation error on the AMPV is then too high which results in an inaccurate impact localization. The same phenomenon is observed by using $\mathcal{F}_2$ and $\mathcal{F}_3$ with at least one modal ponderation inaccurately estimated.

On the opposite, Figure 16 shows the frequency contents of measured and predicted acceleration data of a hard impact that is accurately localized with $\mathcal{F}_4$ but not with $\mathcal{F}_1$. It can be seen that the ponderation of ϕ_1 is not accurately estimated by using $\mathcal{F}_1$, which explains the inaccurate localization. The whole frequency band [85,560]Hz is however accurately reconstructed by using $\mathcal{F}_4$.

The essential difference between impacts applied with the rubber tip and the other tips is the impact duration ($\approx$ 5ms with the rubber tip and $<$ 2ms with the other tips). It is well-known that the shorter the impact duration, the wider the frequency spectrum (compare Figures 15 and 16). Consequently, more modes must be kept in the analysis to identify impacts with a very short duration. However, if too many vibration modes are kept in the analysis then the condition number of the matrices $\mathbf{A}$ increases (see section 4.2), which deteriorates the robustness of the procedure.

In conclusion, as frequently observed with inverse problems [2], there is a trade-off to be found on the number of modes to be kept in the analysis: adding modes increases the expected accuracy of the results, but it decreases the robustness of the procedure. The proposed technique could be improved by iterating on the number of modes to get an optimal reconstruction of the measured data.

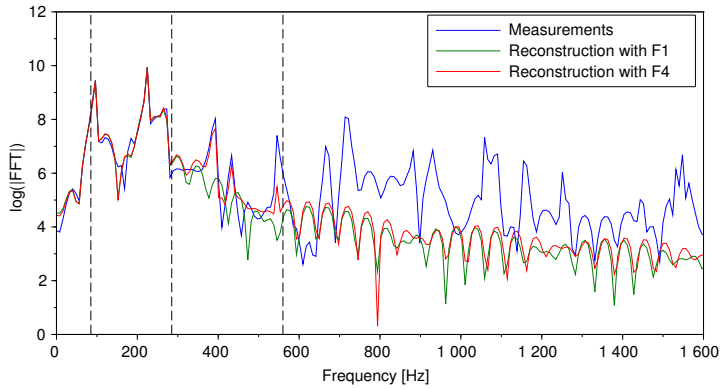

Figure 15: Frequency content reconstruction (soft impact).

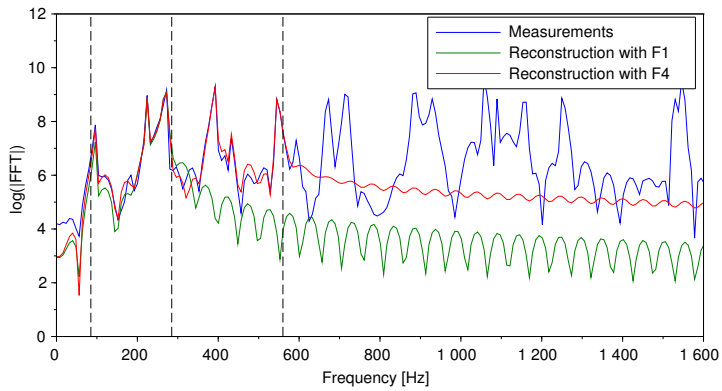

Figure 16: Frequency content reconstruction (hard impact).

6.2. Localization performances depending on impact location

Figure 9 indicates that impacts applied near the center of the plate are more accurately localized than impacts applied near the edges (especially near the corners). This can be explained by plotting the robustness angular maps $M \mapsto \theta_\epsilon(M)$ with $\mathcal{F}_1$ and $\mathcal{F}_4$ (see section 4.1).

Depending on the impact location F, the maximum admissible collinearity tolerance $\theta_\epsilon(F)$ is not the same. Figure 17a confirms that more estimation error is allowed on modal ponderations for impacts applied near the center. Indeed, θ_ϵ drops from 37° in the center of the plate to 3° on a corner. In other words, the signature of an impact, in terms of modal ponderations, is easier to be identified if the impact is applied near the center.

Figure 17b shows the same map with $\mathcal{F}_4$. The trend is similar with higher values of θ_ϵ near the center, and lower values near the corners. The values of θ_ϵ are globally higher in a larger area, with a range between 7° and 39°. As a result, more estimation error is *a priori* allowable by adding modes in the analysis. This could explain the better localization performances with $\mathcal{F}_4$ than $\mathcal{F}_1$ (see Table 3). The exception is the rubber tip that does not sufficiently excite high order modes (see Figure 15), hence their ponderations are not estimated accurately enough.

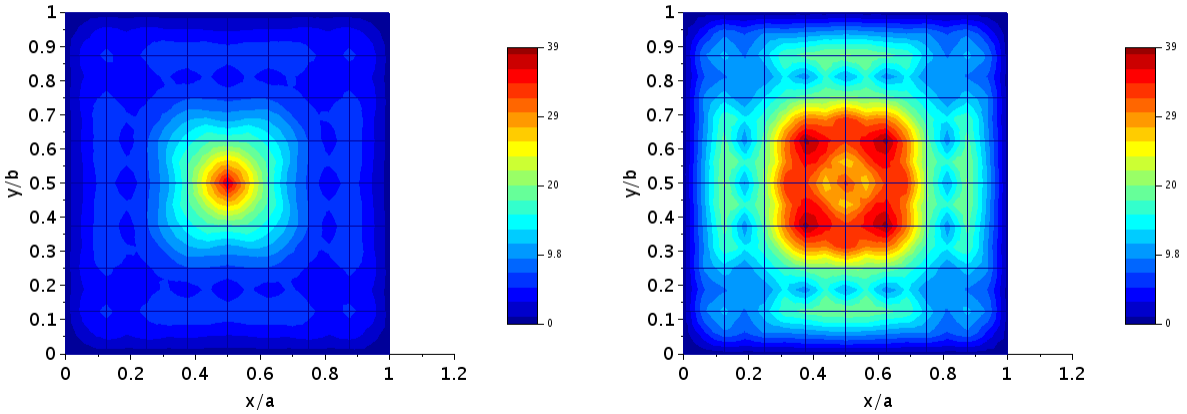

(a) $\mathcal{F}_1$ (b) $\mathcal{F}_4$

Figure 17: Angular Robustness Map $M \mapsto \theta_\epsilon(M)$ (in °) depending on modes selection.

6.3. Computational efficiency

The proposed approach intends to provide a fast and robust procedure for impact identification from vibration measurements. Three quantities can be considered to assess the efficiency of a numerical procedure: the size of required input data, the number of unknowns to be identified, and the computation time.

The inputs of the proposed technique are the measurements of one accelerometer and a reduced number of vibration modes. Three reasons can explain the experimental validation of this approach with this plate. Firstly, the dimensions of the plate are small. As a result, the impact time is correctly estimated with the trigger technique (31). There is no need to consider the impact time as an additional parameter of the load history model, which avoids finding multiple local minima of the distance (9). A larger structure would probably require using more sensors, especially to detect the impact time more accurately. Secondly, measurements were performed in laboratory conditions. In a noisy environment, it could be necessary to apply a band-pass filter to remove the offsets and the high frequency noise. Thirdly, the vibration modes of the plate are analytically known, which eased the experimental modal analysis of the plate. However, it can be appreciated that the procedure described in Figure 6 can be adapted for more complex structures. The challenge is to identify discriminating mode shapes and to determine the associated modal properties (natural frequency, damping ratio and modal mass).

The number of unknowns for the localization problem are the ponderations of the discriminating vibration modes. With the plate, the three first vibration modes form a global DMF. Consequently, the localization problem is reduced to the identification of three modal ponderations only. Regarding the reconstruction problem, the unknowns are the parameters of the selected load history model. Instead of identifying the load history at each sample time [3, 4, 6, 7, 27], the proposed approach consists in capturing specific impact parameters. However, the selected load history model should correctly represent the applied load history. In the proposed application, HS model is found to be the more reliable one in capturing the main peak properties of the load history (impact time and duration).

The exploration of the impact parameters space may be time consuming if the number of parameters is important. A solution could be to use a Genetic Algorithm, or a Particle Swarm Optimization technique [28], in order to automatically select sensitive areas in the impact parameters space. A trade-off is to be found between the accuracy of the reconstruction and the available time to identify the impact event.

7. Conclusion

This paper presents an efficient technique for identifying impact events from vibration measurements of a single point on the structure. The localization problem is addressed by identifying the contributions of specific vibration modes in the response as a signature of impact location. The robustness of the modal ponderations estimation is increased by positioning the sensor on a neutral point of the selected vibration modes family. The force reconstruction problem is addressed by fitting a parametric load history model. A least-squares procedure is proposed to estimate the main load parameters such as the impact time, its duration and its intensity. The number of unknowns is significantly reduced with this technique, which leads to short computation time and increased robustness. The proposed approach is experimentally validated on a simply supported plate equipped with one accelerometer only. Results demonstrate an accurate localization of the impact points and an effective load history reconstruction when the selected load model correctly represents the applied force.

The same formalism could be applied for a more complex structure. The challenge is to identify a discriminating vibration modes family to make the reverse link between the modal ponderations and the impact point. Work is in progress to experimentally validate this impact identification technique on a large composite stiffened aircraft panel.

8. Acknowledgments

The first author thanks the french National Association of Research and Technology for his support through a PhD grant (n°2016/0887). The authors are also thankful to the mathematician Prof. Saab Abou-Jaoude for all his valuable ideas.

References

[1] H. Inoue, J. Harrigan, S. Reid, Review of inverse analysis for indirect measurement of impact force, Applied Mechanics Reviews 54(6) (2001) 503–524.
[2] P. Hansen, Rank-deficient and discrete ill-posed problems: numerical aspects of linear inversion, SIAM, 1998.
[3] Q. Leclère, C. Pezerat, B. Laulagnet, L. Polac, Indirect measurement of main bearing loads in an operating diesel engine, Journal of Sound and Vibration 286(1-2) (2005) 341–361.
[4] K. Khalori, L. Ye, S. Mustapha, J. Li, B. Li, Reconstruction and analysis of impact forces on a steel-beam-reinforced concrete deck, Experimental Mechanics 56(9) (2016) 1547–1558.
[5] P. Hansen, Analysis of discrete ill-posed problems by means of the L-curve, Journal of the Society for Industrial and Applied Mathematics 34(4) (1992) 561–580.
[6] Z. Boukria, P. Perrotin, A. Bennani, A. Limam, Identification et localisation des impacts par analyse inverse - Poutre et plaque -, in: 19ème Congrès Français de Mécanique, 2009.
[7] R. Zemcik, J. Bartosek, Z. Lasova, T. Kroupa, Reconstruction of impact on composite airfoil segment using piezoelectric sensors, in: Proceedings of 7th EWSHM, 2014.
[8] B.-T. Wang, C.-H. Chiu, Determination of unknown impact force acting on a simply supported beam, Mechanical Systems and Signal Processing 17(3) (2003) 683–704.
[9] G. Yan, L. Zhou, Impact load identification of composite structure using genetic algorithms, Journal of sound and vibration 319(3-5) (2009) 869–884.
[10] B. Qiao, X. Chen, X. Xue, X. Luo, R. Liu, The application of cubic B-spline collocation method in impact force identification, Mechanical Systems and Signal Processing 64-65 (2015) 413–427.
[11] S. Ahmari, M. Yang, Impact location and load identification through inverse analysis with bounded uncertain measurements, Smart Materials and Structures 22(8) (2013) 085024.
[12] J. Frieden, J. Cugnoni, J. Botsis, T. Gmür, Low energy impact damage monitoring of composites using dynamic strain signals from fbg sensors – part i: Impact detection and localization, Composite Structures 94(2) (2012) 438–445.
[13] G. Zhao, H. Hu, S. Li, L. Liu, K. Li, Localization of impact on composite plates based on integrated wavelet transform and hybrid minimization algorithm, Composite Structures 176 (2017) 234–243.
[14] Q. Li, Q. Lu, Impact localization and identification under a constrained optimization scheme, Journal of Sound and Vibration 366 (2016) 133–148.
[15] L. Vladislav, R. Zemcik, T. Kroupa, J. Bartosek, Reconstruction of impact force on curved panel using piezoelectric sensors, Procedia Engineering 48 (2012) 367–374.
[16] A. El-Bakari, A. Khamlichi, E. Jacquelin, R. Dkiouak, Assessing impact force localization by using a particle swarm optimization algorithm, Journal of Sound and Vibration 333(6) (2014) 1554–1561.

[17] J. Briggs, M.-K. Tse, Impact force identification using extracted modal parameters and pattern matching, International Journal of Impact Engineering 12(3) (1991) 361–372.
[18] B.-T. Wang, Prediction of impact and harmonic forces acting on arbitrary structures: theoretical formulation, Mechanical Systems and Signal Processing 16(6) (2002) 935–953.
[19] Y. Zhong, J. Xiang, H. Gao, Y. Zhou, Impact energy level assessment of composite structures using MUSIC-ANN approach, Structural Control and Health Monitoring 23 (2016) 825–837.
[20] M. Ruiz, L. Mujica, X. Berjaga, J. Rodellar, Partial least square/projection to latent structures (PLS) regression to estimate impact localization in structures, Smart Materials and Structures 22 (2013) 025028.
[21] M. Yang, S. Ahmari, M. Selekwa, Impact event identification in thin plates through real strain measurements, Structural Control and Health Monitoring 24(7) (2016) 1–14.
[22] M. Géradin, D. J. Rixen, Mechanical Vibrations - Theory and Application to Structural Dynamics, Third Edition, Wiley, 2015.
[23] U. M. S. Choudhary, Fundamental limits of blind deconvolution part I : Ambiguity kernel, in: IEEE Global Conference on Signal and Information Processing (GlobalSIP), 2014.
[24] D. Goutaudier, Impact identification technique for a structure with weakly damped and well-separated low frequency vibration modes, PhD thesis, Conservatoire National des Arts et Métiers de Paris, 2019.
[25] A. Leissa, Vibration of plates, NASA SP-160, 1969.
[26] O. Robin, J.-D. Chazot, R. Boulandet, M. Michau, A. Berry, N. Atalla, A plane and thin panel for representative simply supported boundary conditions for laboratory vibroacoustic tests, Acta Acustica United with Acustica 102(1) (2016) 170–182.
[27] J. Park, S. Ha, F.-K. Chang, Monitoring impact events using a system-identification method, AIAA Journal 47(9) (2009) 2011–2021.
[28] R. Eberhart, Y. Shi, J. Kennedy, Swarm intelligence, Morgan Kaufmann, 2001.